Journal of Solid State Chemistry 185 (2012) 191–197

Contents lists available at SciVerse ScienceDirect

Journal of Solid State Chemistry

journal homepage: www.elsevier.com/locate/jssc

Synthesis and characterization of a nanocomposite of goethite nanorods and reduced graphene oxide for electrochemical capacitors

Qingliang Shou [a], Jipeng Cheng [a,*], Li Zhang [b,*], Bradley J. Nelson [b], Xiaobin Zhang [a]

[a] State Key Laboratory of Silicon Materials, Department of Materials Science and Engineering, Zhejiang University, Hangzhou 310027, China
[b] Institute of Robotics and Intelligent Systems, ETH Zurich, CH-8092 Zurich, Switzerland

ARTICLE INFO

Article history:
Received 24 September 2011
Received in revised form
9 November 2011
Accepted 11 November 2011
Available online 19 November 2011

Keywords:
Nanocomposites
Goethite
Nanorods
Reduced graphene oxide
Electrochemical capacitance

ABSTRACT

We report a one-step synthesis of a nanocomposite of goethite (α-FeOOH) nanorods and reduced graphene oxide (RGO) using a solution method in which ferrous cations serve as a reducing agent of graphite oxide (GO) to graphene and a precursor to grow goethite nanorods. As-prepared goethite nanorods have an average length of 200 nm and a diameter of 30 nm and are densely attached on both sides of the RGO sheets. The electrochemical properties of the nanocomposite were characterized by cyclic voltammetry (CV) and chronopotentiometry (CP) charge–discharge tests. The results showed that goethite/RGO composites have a high electrochemical capacitance of 165.5 F g^{-1} with an excellent recycling capability making the material promising for electrochemical capacitors.

1. Introduction

Electrochemical capacitors are important electronic devices because of their high capacitance and the possibility to couple them with batteries to provide pulses of peak power during acceleration and on uphill gradients [1]. Carbon-based materials and transition metal oxides are considered to be promising materials for electrical double-layer capacitors and pseudocapacitors, respectively. Many efforts have focused on the preparation of metal oxide/carbon nanotube composites because of their good performance as electrode materials for supercapacitors [2–5]. Graphene, a two-dimensional monolayer of carbon atoms, has captured enormous attention since its discovery in 2004 [6], because it possesses unique properties, such as superior electrical conductivity, large specific surface area, strong mechanical stability, and chemical tolerance, indicating it could act as a possible substitute for carbon nanotubes in various nanocomposites.

Fe_3O_4, Fe_2O_3, and FeOOH have recently attracted great interests due to their natural abundance and eco-friendliness [7,8]. For portable energy storage systems several groups reported nanocomposites of iron oxide and graphene as electrodes of lithium ion battery [9–12]. Goethite (α-FeOOH) has potential applications in many fields such as electrode materials [13], catalysts [14], adsorption of arsenite [15], and magnetic materials [16]. Though there has been report utilizing β-FeOOH as electrode material for supercapacitor [17], up to now, the possibility of goethite/graphene as electrode materials for electrochemical capacitors has never been explored.

Generally, pure graphene is seldom used as a raw material to produce graphene-based nanocomposites due to its poor dispersibility in solvents. Alternatively, graphite oxide (GO) has inherent oxygen-contained functional groups and can form stable colloidal suspensions in polar solvents [18]. Thus, GO is preferred in the reported synthesis methods of iron oxide/graphene composites [9–12]. Nevertheless, those methods required the introduction of additional hazardous reductants, or a following reduction process, which were either tedious or time consuming. Therefore, it merits considerable efforts to explore green and facile ways to produce homogeneous irons/graphene composites.

In this paper, we present an alternative method to synthesize a composite of goethite nanorods and reduced graphene oxide (RGO) by combining the growth of FeOOH nanorods and the reduction of GO in one step. The reducing capability of ferrous ions was studied through Fourier transform infrared (FT-IR) spectra and ultraviolet-visible (UV–vis) absorption spectra. The structure and morphology of the as-prepared nanocomposites were characterized by X-ray diffraction (XRD), scanning electron microscope (SEM), and transmission electron microscope (TEM). The electrochemical properties of the nanocomposites were investigated by cyclic voltammetry (CV) and chronopotentiometry (CP) charge–discharge tests. The results reveal that goethite

* Corresponding authors. Fax: +86 571 8795 1411.
E-mail addresses: chengjp@zju.edu.cn (J. Cheng), lizhang@ethz.ch (L. Zhang).

0022-4596/$ - see front matter © 2011 Elsevier Inc. All rights reserved.
doi:10.1016/j.jssc.2011.11.020

nanorod/RGO composites are promising electrode materials for electrochemical capacitors and other energy storage applications.

2. Experimental

2.1. Preparation of goethite nanorods-RGO nanocomposite

The graphite oxide (GO) used in this study was prepared from natural graphite by the Hummers method as reported in Refs. [19,20]. Goethite nanorod/RGO composites were prepared by a solution approach. In a typical process, 0.2 g GO was exfoliated by sonication in 100 mL distilled water. Separately, 2.78 g $FeSO_4 \cdot H_2O$ and 4 g CH_3COONa were dissolved into 50 mL water, and the ferrous solution was subsequently added into the GO suspension. The suspension was sonicated for 1 h at room temperature, and refluxed for another 2 h. After the reaction, the solution was allowed to cool to room temperature, and the resulting product was separated by filtration, and then washed with distilled water and ethanol. The final product was dried in vacuum at 60 °C for 12 h. In the current process, CH_3COONa was used as the source of hydroxide ions during the hydrolysis of iron salts to form iron oxyhydroxide (FeOOH) [21]. For comparison, pure RGO without goethite was also prepared via a similar procedure in the absence of CH_3COONa.

2.2. Microstructural characterization

The phase and composition of the products were characterized by Powder XRD (X'Pert PRO). The measurements of the FT-IR spectra and the UV–vis absorption spectra of the samples were performed by a Bruker spectrometer (TENSOR 27) and a UV–vis spectrophotometer (Shanghai Spectrophotometer Factory, China), respectively. The morphology and structure of the products were investigated by a field emission scanning electron microscope (FESEM, Hitachi S-4800) and a transmission electron microscope (TEM, Philips CM-200).

2.3. Electrochemical characterization

The electrochemical charge–discharge performance of the composites was evaluated in a 1M Na_2SO_3 solution by cyclic voltammetry (CV) and chronopotentiometry (CP). To prepare working electrodes, slurries made by goethite nanorod/RGO composites were used as the electroactive material, acetylene black as the conductive agent, and polyvinylidene fluoride (PVDF) as the binder. They were mixed in a weight ratio of 80:10:10 in *N*-methyl-2-pyrrolidone solvent and coated on a square-shaped nickel foam substrate (1 cm × 1 cm). The active material loaded on the electrode was approximately 5 mg on each electrode. Before the electrochemical test, the electrode was soaked in 1 M Na_2SO_3 solution overnight. Electrochemical characterization was carried out in a three-electrode system with 1 Na_2SO_3 aqueous solution as the electrolyte. A platinum foil and a saturated calomel electrode (SCE) were applied as the counter and reference electrodes, respectively. The specific capacitance can be obtained from the CV curves according to

$$C_s = \frac{\int IdV}{vm\Delta V} \quad (1)$$

or from the charge–discharge curves according to

$$C_s = \frac{I\Delta t}{m\Delta V} \quad (2)$$

where C_s is the specific capacitance (F g^{-1}), I is the current, V is the potential vs. SEC, ΔV is the voltage difference, v is the potential scan rate (mV s^{-1}), m is the mass of the electroactive materials in the electrodes (g), and Δt is the discharging time (s).

3. Results and discussion

Unlike previous preparation methods of iron oxide/RGO composites, which required the introduction of a reducing agent such as hydrazine hydrate to reduce GO into RGO [11,22], ferrous ions acted as both a reducing agent and an iron source for the formation of goethite in the current procedure. To examine the reduction of GO by Fe^{2+}, a control experiment without the addition of CH_3COONa was carried out to obtain pure RGO without goethite. FT-IR spectra of GO, RGO and goethite nanorods/RGO composite are shown in Fig. 1a. The curve of GO shows a stretching vibration of C═O at 1720 cm^{-1}, and two peaks at 3420 cm^{-1} and 1390 cm^{-1} corresponding to the stretching vibration and deformation vibration of O–H. The spectrum also shows two peaks at 1078 cm^{-1} and 1234 cm^{-1} originated from the C–O stretching vibrations of alkoxy. The peak at 1627 cm^{-1} is assigned to the vibrations of the adsorbed water molecules and the contributions from the vibration of aromatic C═C [23]. For the RGO curve, the bands associated with oxygen-containing functional groups significantly decrease,

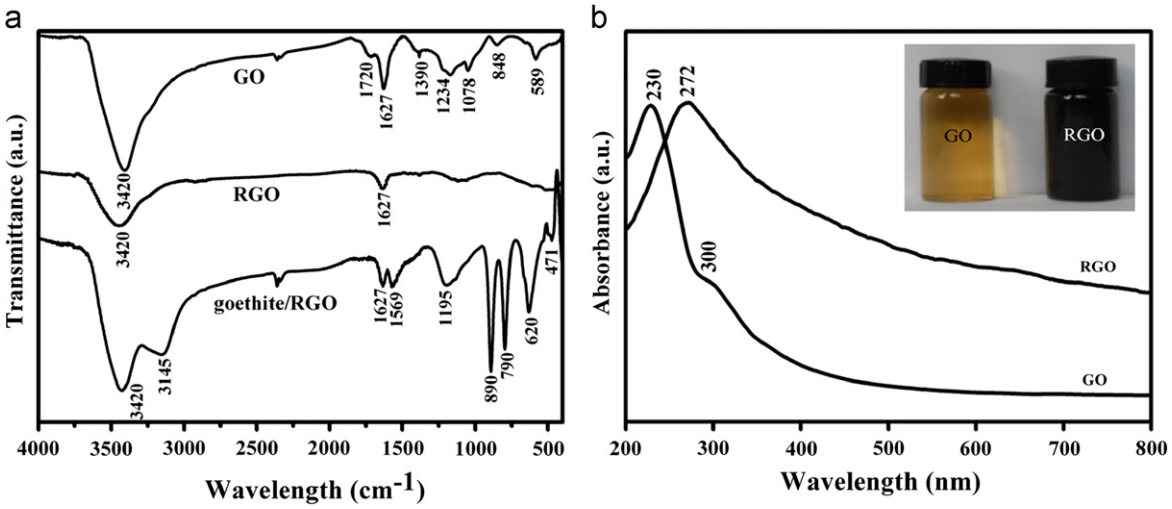

Fig. 1. (a) FT-IR spectra of GO, RGO and goethite/RGO composite. Compared with GO, most of the peaks related to oxygen-containing groups in RGO disappeared. (b) UV–vis spectra of GO and RGO. RGO shows a redshift from 230 to 272 nm, suggesting the restoration of the π electronic conjugation within graphene sheets.

and some of them even disappear. These results validate an effective removal of the oxygen-containing groups in GO by the reduction of Fe^{2+}. The FT-IR curve of goethite/RGO composite indicates the formation of FeOOH in the composite, since the main absorption bands are in good agreement with that of standard spectrum of FeOOH [24,25].

Fig. 1b shows the UV–vis spectra of GO and RGO dispersed in water. The spectra of GO shows a high peak at 230 nm corresponding to the $\pi \rightarrow \pi^*$ transition of aromatic C–C bonds and a small shoulder at 300 nm, which can be attributed to the $n \rightarrow \pi^*$ transition of C=O bonds [26]. Only an intensive peak is observed at 272 nm for RGO, and the shoulder peak near 300 nm disappears. The redshift of absorption band of RGO from 230 to 272 nm suggests the restoration of the π electronic conjugation within graphene sheets after Fe^{2+} treatment [27]. The reduction of GO is clearly indicated by the color change of the aqueous dispersion of GO and RGO from yellow to black, the natural color of graphite, as shown in the inset of Fig. 1b.

Fig. 2 shows the XRD patterns of GO, RGO and goethite/RGO composites. The intensive peak at around $2\theta = 10^\circ$ (curve "a" in Fig. 2) corresponds to the (0 0 1) reflection of GO [28,29]. The d-spacing of GO (0.90 nm) estimated from the Bragg equation is much larger than that of the graphite (0 0 2) reflection (about 0.34 nm) due to the introduction of oxygen-containing functional groups on the graphene sheets of GO during the oxidation process. In contrast, in the diffraction pattern of RGO (curve "b" in Fig. 2), the disappearance of the peak at $2\theta = 10^\circ$ provides further evidence for the reduction of GO. The diagram of RGO shows a broad peak near 23° corresponding to graphite (0 0 2) interlayer d-spacing of 0.38 nm, which is consistent with a highly reduced product [30]. The result implies that most of the oxygen-containing functional groups are removed in the process [31]. In addition, the broadening of the reflection peak indicates thin layers formed in the *c* axis of the graphite structure or a poor crystallinity of the product along the stacking direction [29,32]. For goethite/RGO composites the major diffraction peak is assigned to the orthorhombic structure of α-FeOOH (JCPDS card No.29-0713) in curve "c" of Fig. 2. The relatively low and broad peak between 10° and 30° confirms the existence of RGO in the composites. This also suggests that significant face-to-face stacking of graphene sheets in the *c* direction of the graphite structure is restricted [33] due to the introduction of goethite nanorods on both sides of the graphene sheets. This is also consistent with the SEM and TEM results (see below). No apparent peaks from other impurities are observed.

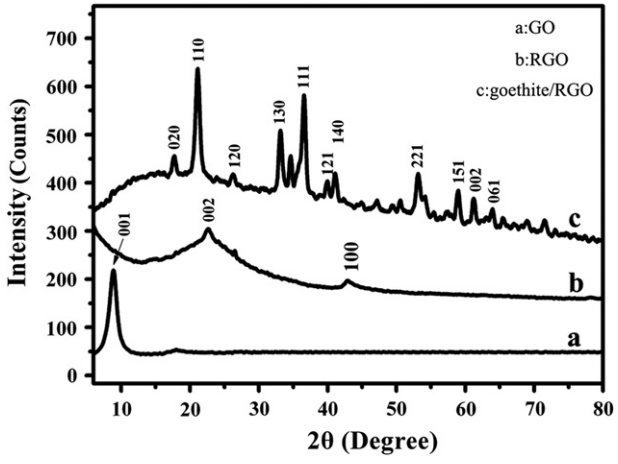

Fig. 2. XRD patterns of GO ("a"), RGO ("b") and the goethite/RGO composite ("c"), showing that the GO is reduced to RGO and goethite is synthesized.

To obtain further information on the surface chemical composition of the goethite/RGO composite, XPS analysis has been carried out. In the wide scan spectrum (Fig. S1, Supplementary Information), photoelectron lines at binding energies of about 284.1 and 530.0 eV are assigned to carbon (C1*s*) and oxygen (O 1*s*), respectively. In Fe 2p high resolution XPS spectrum (inset of Fig. S1), the binding energy peaks at 711.2 and 724.4 eV are corresponding to Fe 2*p*3/2 and Fe 2*p*1/2, respectively, which are very close to the values of α-FeOOH published in the literature [34]. Moreover, Fe 2*p*3/2 satellite peak is found at 719.3 eV, similar to other iron oxide samples of only Fe^{3+} states [11].

The TEM micrograph and SAED pattern (inset) of GO reveal that GO has a wrinkled membrane-like structure, as shown in Fig. 3a. The SAED pattern in the *c* direction of GO shows a hexagonal structure with the AB stacking order [35]. SEM and TEM micrographs of the goethite/RGO composite are shown in Fig. 3(b–d), in which the goethite exhibits a rod-like morphology with an average length of 200 nm and a diameter of 30 nm densely attached on both sides of the graphene sheets. It can be seen that even after a long duration of sonication during the preparation of the TEM and SEM specimen, FeOOH nanorods are still anchored on the surface of RGO sheets, revealing a strong interaction between FeOOH nanorods and RGO sheets. High resolution TEM (HRTEM) micrograph of one goethite nanorod is shown in Fig. 3e. The (1 1 0) plane of goethite crystal can be identified from the d-spacing of 4.23 Å, which is consistent with the XRD result. Meanwhile, according to the elemental distribution of carbon, oxygen, and iron obtained by EDS elemental mapping as shown in Fig. 4, the goethite nanorods are uniformly dispersed in the composite.

To investigate the evolution of the goethite/RGO composite in the process, time-dependent experiments were conducted, during which samples with different refluxing times were collected and inspected using an SEM. At the initial stage, i.e. the sample for a 5 min reaction, nanoparticles with a diameter of approximate 10 nm were formed on the surface of the graphene sheets as shown in Fig. 5a. A small fraction of elongated particles was also observed at this stage. As the reaction time proceeded to 30 min (Fig. 5b) the nanoparticles grew to form nanorods and adjacent rods began to bind, whereas the lengths and diameters of the nanorods varied. When the reaction time reached 60 min (Fig. 5c), the nanorods exhibited increased lengths and diameters. When the reaction time was set to 120 min (Fig. 5d), almost no nanoparticles remained and the sample was composed of rod-like nanostructure with a uniform length and diameter. Based on the above results, a formation process of goethite/RGO is schematically illustrated in Fig. 5(e). In the step (I), Fe^{2+} was bonded on the negatively charged surface of GO sheets by electrostatic interactions. In the step (II), goethite crystal nuclei formed by the reaction of Fe^{2+} with GO and OH^- produced by the hydrolysis of CH_3COO^-. Eventually, in the third step (III) many neighboring nuclei grew into rod-like crystals through oriented aggregation to reduce their surface energy [21,36,37].

In the CV tests the electrodes were prepared by goethite nanorod/RGO composite and different scanning rates within a potential window of −0.85 to 0.1 V (vs. SCE) were applied. The CV curves are shown in Fig. 6. The shape of the CV curves indicate that the capacitance characteristic of the goethite/RGO composite is distinct from that of the electric double-layer capacitance, which would produce a rectangle-like curve. Oxidative peaks can be clearly observed in our CV measurements. The asymmetry of the curves is most likely due to the combination of the double layer capacitance from RGO and pseudo-capacitances from FeOOH contributing to the total capacitance. The pseudo-capacitance reaction mechanisms of FeOOH in a Na_2SO_3 solution may result from the surface redox reaction of sulfur in the form of

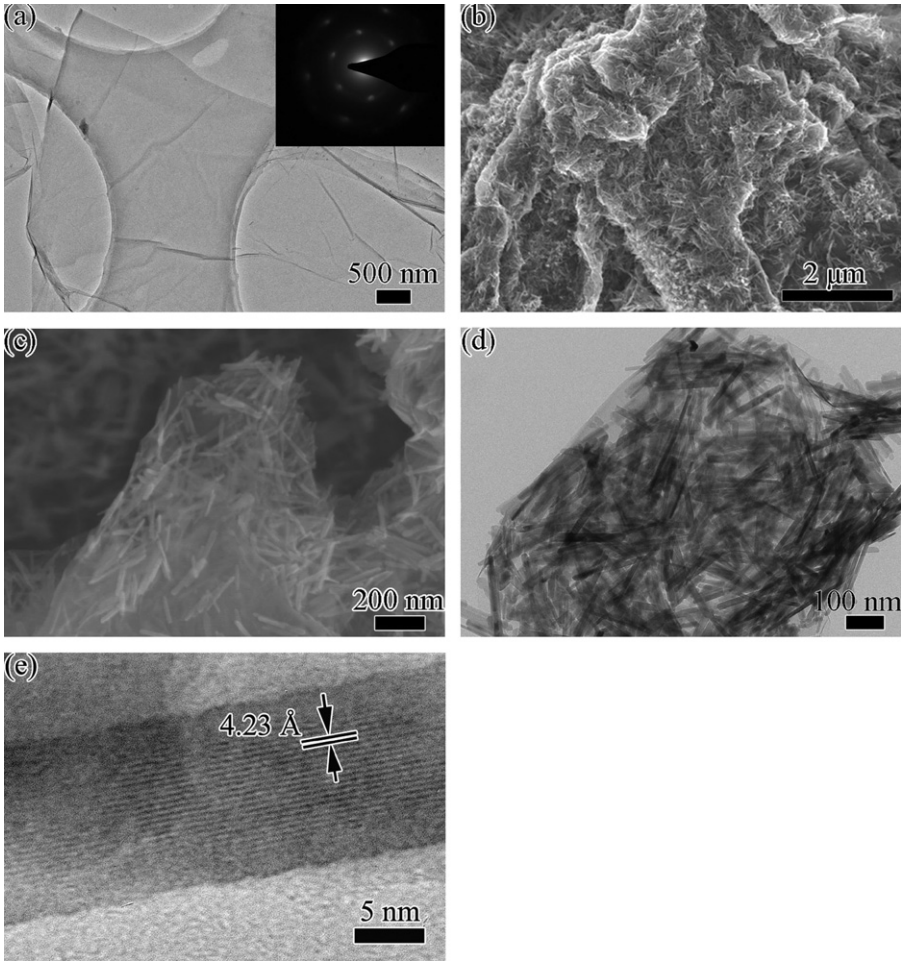

Fig. 3. (a) TEM and SAED micrographs of GO, SEM (b, c) and TEM (d) of goethite/RGO showing goethite nanorods uniformly distributed on RGO sheets, and HRTEM micrograph of one goethite nanorod (e).

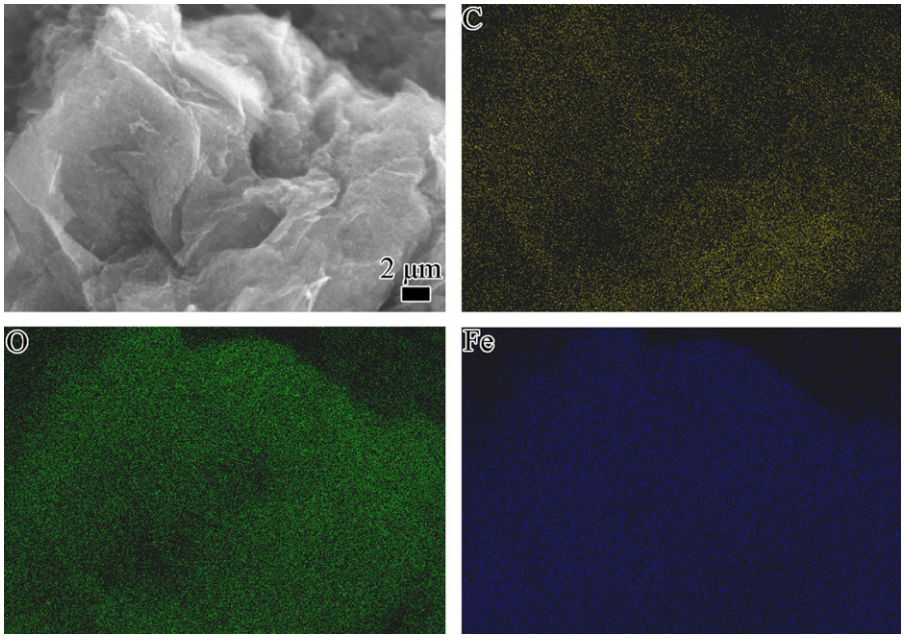

Fig. 4. SEM micrograph and corresponding carbon, oxygen, and iron distribution of goethite/RGO composites obtained from EDS elemental mapping. The elemental mapping indicates uniform dispersion of goethite in the composite.

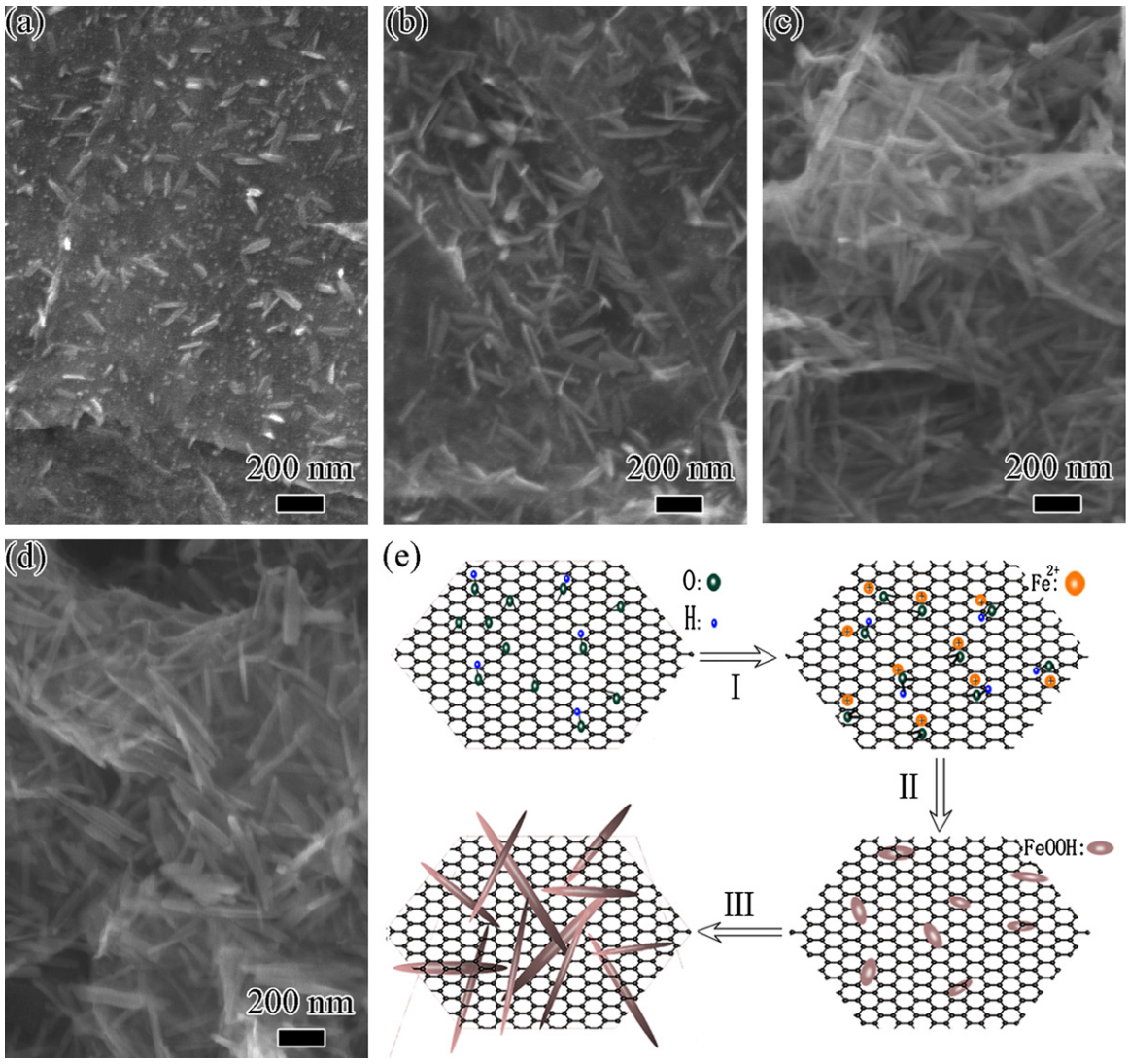

Fig. 5. SEM micrographs of time-dependent samples after refluxing for (a) 5 min; (b) 30 min; (c) 60 min; (d) 120 min, and (e) schematic illustration for the formation process of goethite/RGO.

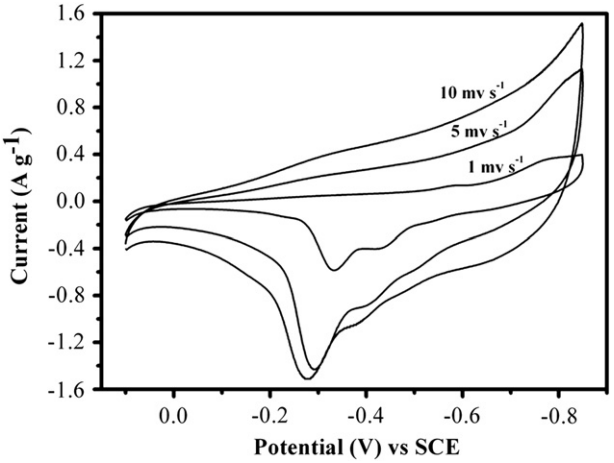

Fig. 6. CV curves at different scan rate: 1, 5, and 10 mV s^{-1}, in which the shape of the CV curves is distinct from that of the electric double-layer capacitance.

sulfate and sulfite anions, as well as the possible redox reactions between Fe^{2+} and Fe^{3+} accompanied by intercalation of sulfite ions to balance the extra charge with the iron oxide layers [38,39]. It is notable that the CV curves retained their configurations with the increase of sweep rate, except that a positive shift of oxidation peaks and a negative shift of reduction peaks are observed, which is mainly due to the resistance of the electrode [28].

The dependence of the specific capacitance of the composite electrode on the scan rate of CV is shown in Fig. 7. The specific capacitance decreases from 165.5 to 44.5 F g^{-1} as the scan rate is increased from 1 to 100 mV s^{-1}. The decrease in specific capacitance is attributed to diffusion limits of electrolyte ions. Only the outer active surface is responsible for charge storage, while the inner active sites cannot sustain the redox transitions. The decrease in capacitance suggests that parts of the surface of the electrode are inaccessible at high charging-discharging rates. Hence, the specific capacitance at the slowest scanning rate is the actual value of the electrode material [40].

To further investigate the capacitive behavior of the goethite/RGO composite, a chronopotentiometry charge–discharge experiment was performed within a potential window of −0.85 to 0.1 V at current density of 0.5, 1, and 2 A g^{-1}, as shown in Fig. 8. The shape of the charge and discharge curves shows the characteristic of the pseudo-capacitance, in good agreement with the result of the CV curve. The specific capacitance values calculated by Eq. (2) are 132, 114, and 73 F g^{-1}, at the current density of 0.5, 1,

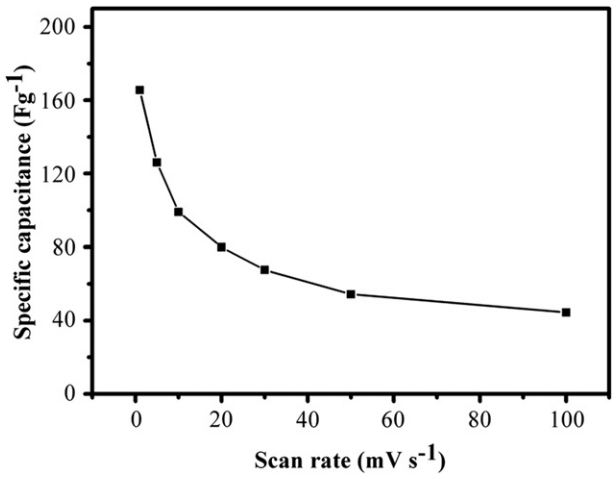

Fig. 7. Dependence of specific capacitance on scanning rate showing a decrease of the specific capacitance with the increasing canning rate.

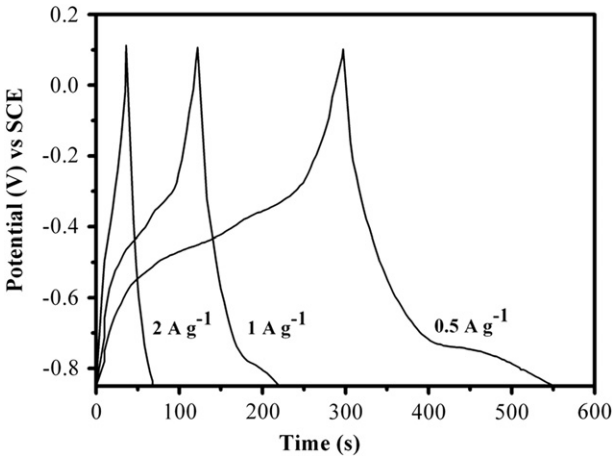

Fig. 8. Charge–discharge curves at different current density: 0.5, 1, and 2 A g^{-1}, showing the characteristic of pseudo-capacitance.

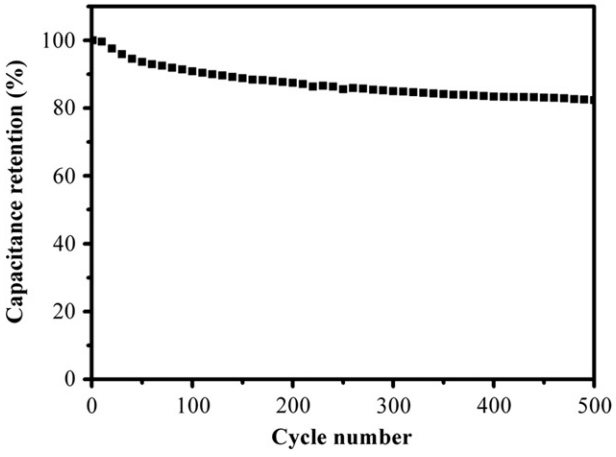

Fig. 9. Cycle-life data of goethite/RGO composite electrode calculated from the CV measurement at 20 mV s^{-1}, showing the specific capacitance remains almost constant after 200 cycles.

and 2 A g^{-1}, respectively. The values are consistent with the calculations from the CV tests. Fig. 9 shows the cyclic performance of the electrode examined by CV test at a scan rate of 20 mV s^{-1} for 500 cycles. There is a 13% decrease in specific capacitance in the first 200 cycles, while the specific capacitance remains almost constant after 200 cycles. A decay of 1.5% is observed between 200 and 500 cycles indicating its excellent recycling capability.

It is important that the composite should have good stability after the CV test for its practical application. SEM and XRD (see Fig. S2 and Fig. S3 in the supporting information) results after CV test reveal that compared with its counterpart before the CV test (Figs. 2c and 3b), there is no obvious change in the nanostructure, indicating the composite possesses good structural stability, which is consistent with the stable cycling performance.

4. Conclusions

A composite of goethite nanorods and reduced graphene oxide (RGO) has been obtained through a one-step solution method, in which RGO and goethite nanorods are formed simultaneously using ferrous cations as the reducing agent and the precursor. The RGO sheets are decorated with goethite nanorods. The as-prepared composite of goethite nanorods and RGO exhibits a high electrochemical capacitance, i.e. 165.5 F g^{-1} in Na_2SO_3 solution, and a good recycling capability, which is promising for supercapacitor applications.

Acknowledgments

We thank the FIRST lab of ETH Zurich for technical support. Funding for this research was partially provided by the open funding (Grant nr. SKL 2009-4) of the State Key Laboratory of Zhejiang University, P. R. China, the Sino-Swiss Science and Technology Cooperation (SSSTC, Grant nr. EG 08-092009) and the opening foundation of Zhejiang Provincial Top Key Discipline (No. 20110905).

Appendix A. Supporting information

Supplementary data associated with this article can be found in the online version at doi:10.1016/j.jssc.2011.11.020.

References

[1] C.Z. Yuan, X.G. Zhang, B. Gao, J. Li, Mater. Chem. Phys. 101 (2007) 148–152.
[2] I.H. Kim, J.H. Kim, K.B. Kim, Electrochem. Solid-State Lett. 8 (2005) A369–A372.
[3] Y. Shan, L. Gao, Mater. Chem. Phys. 103 (2007) 206–210.
[4] Y.Z. Zheng, M.L. Zhang, P. Gao, Mater. Res. Bull. 42 (2007) 1740–1747.
[5] Y.K. Zhou, B.L. He, F.B. Zhang, H.L. Li, J. Solid State Electrochem. 8 (2004) 482–487.
[6] K.S. Novoselov, A.K. Geim, S.V. Morozov, D. Jiang, Y. Zhang, S.V. Dubonos, I.V. Grigorieva, A.A. Firsov, Science 306 (2004) 666–669.
[7] J.P. Cheng, X.B. Zhang, G.F. Yi, Y. Ye, M.S. Xia, J. Alloys Compd. 455 (2008) 5–9.
[8] D. Shi, J.P. Cheng, F. Liu, X.B. Zhang, J. Alloys Compd. 502 (2010) 365–370.
[9] P.C. Lian, X.F. Zhu, H.F. Xiang, Z. Li, W.S. Yang, H.H. Wang, Electrochim. Acta 56 (2010) 834–840.
[10] M. Zhang, D.N. Lei, X.M. Yin, L.B. Chen, Q.H. Li, Y.G. Wang, T.H. Wang, J. Mater. Chem. 20 (2010) 5538–5543.
[11] X.J. Zhu, Y.W. Zhu, S. Murali, M.D. Stollers, R.S. Ruoff, Acs Nano 5 (2011) 3333–3338.
[12] G. Zhou, D. Wang, F. Li, L. Zhang, N. Li, Z. Wu, L. Wen, G.Q. Lu, H. Cheng, Chem. Mater. 22 (2010) 5306–5313.
[13] K.S. Hwang, T.H. Yoon, C.W. Lee, Y.S. Son, J.K. Hwang, J. Power Sources 75 (1998) 13–18.
[14] J.F. Boily, N. Nilsson, P. Persson, S. Sjoberg, Langmuir 16 (2000) 5719–5729.
[15] G. Ona-Nguema, G. Morin, F. Juillot, G. Calas, G.E. Brown, Environ. Sci. Technol. 39 (2005) 9147–9155.
[16] B.J. Lemaire, P. Davidson, J. Ferre, J.P. Jamet, P. Panine, I. Dozov, J.P. Jolivet, Phys. Rev. Lett. 88 (2002) 125507.

[17] W.H. Jin, G.T. Cao, J.Y. Sun, J. Power Sources 175 (2008) 686–691.
[18] H. He, C. Gao, ACS Appl. Mater. Interfaces 2 (2010) 3201–3210.
[19] W.S. Hummers, R.E. Offeman, J. Am. Chem. Soc. 80 (1958) 1339-1339.
[20] Z.S. Wu, W.C. Ren, L.B. Gao, B.L. Liu, C.B. Jiang, H.M. Cheng, Carbon 47 (2009) 493–499.
[21] Y. Wang, J.L. Cao, S.R. Wang, X.Z. Guo, J. Zhang, H.J. Xia, S.M. Zhang, S.H. Wu, J. Phys. Chem. C 112 (2008) 17804–17808.
[22] X.P. Shen, J.L. Wu, S. Bai, H. Zhou, J. Alloys Compd. 506 (2010) 136–140.
[23] Y.X. Xu, H. Bai, G.W. Lu, C. Li, G.Q. Shi, J. Am. Chem. Soc. 130 (2008) 5856–5857.
[24] F.X. Geng, Z.G. Zhao, J.X. Geng, H.T. Cong, H.M. Cheng, Mater. Lett. 61 (2007) 4794–4796.
[25] P. Ou, G. Xu, Z.H. Ren, X.H. Hou, G.R. Han, Mater. Lett. 62 (2008) 914–917.
[26] J.I. Paredes, S. Villar-Rodil, A. Martinez-Alonso, J.M.D. Tascon, Langmuir 24 (2008) 10560–10564.
[27] D. Li, M.B. Muller, S. Gilje, R.B. Kaner, G.G. Wallace, Nat. Nanotechnol. 3 (2008) 101–105.
[28] J. Yan, T. Wei, W.M. Qiao, B. Shao, Q.K. Zhao, L.J. Zhang, Z.J. Fan, Electrochim. Acta 55 (2010) 6973–6978.
[29] A.V. Murugan, T. Muraliganth, A. Manthiram, Chem. Mater. 21 (2009) 5004–5006.
[30] D.R. Dreyer, S. Murali, Y.W. Zhu, R.S. Ruoff, C.W. Bielawski, J. Mater. Chem. 21 (2011) 3443–3447.
[31] H.J. Shin, K.K. Kim, A. Benayad, S.M. Yoon, H.K. Park, I.S. Jung, M.H. Jin, H.K. Jeong, J.M. Kim, J.Y. Choi, Y.H. Lee, Adv. Funct. Mater. 19 (2009) 1987–1992.
[32] J.F. Shen, B. Yan, M. Shi, H.W. Ma, N. Li, M.X. Ye, J. Mater. Chem. 21 (2011) 3415–3421.
[33] Y.C. Si, E.T. Samulski, Chem. Mater. 20 (2008) 6792–6797.
[34] L. Martinez, D. Leinen, F. Martin, M. Gabas, J.R. Ramos-Barrado, E. Quagliata, E.A. Dalchiele, J. Electrochem. Soc. 154 (2007) D126–D133.
[35] H.K. Jeong, Y.P. Lee, R.J.W.E. Lahaye, M.H. Park, K.H. An, I.J. Kim, C.W. Yang, C.Y. Park, R.S. Ruoff, Y.H. Lee, J. Am. Chem. Soc. 130 (2008) 1362–1366.
[36] B. Tang, G.L. Wang, L.H. Zhuo, J.C. Ge, L.J. Cui, Inorg. Chem. 45 (2006) 5196–5200.
[37] Q.Y. Hao, S.A. Liu, X.M. Yin, Y.G. Wang, Q.H. Li, T.H. Wang, Solid State Sci. 12 (2010) 2125–2129.
[38] N.L. Wu, S.Y. Wang, C.Y. Han, D.S. Wu, L.R. Shiue, J. Power Sources 113 (2003) 173–178.
[39] Y.H. Kim, S.J. Park, Curr. Appl. Phys. 11 (2011) 462–466.
[40] T.P. Gujar, V.R. Shinde, C.D. Lokhande, W.-Y. Kim, K.-D. Jung, O.-S. Joo, Electrochem. Commun. 9 (2007) 504–510.